

# The Sensitivity of $r$ -Process Nucleosynthesis to Individual $\beta$ -Delayed Neutron Emission Probabilities

Rebecca SURMAN, Matthew MUMPOWER, and Ani APRAHAMIAN

*Department of Physics, University of Notre Dame, Notre Dame, IN 46656, USA*

*E-mail: rsurman@nd.edu*

(Received September 30, 2014)

Simulations of rapid neutron capture, or  $r$ -process, nucleosynthesis are sensitive to the nuclear physics inputs for thousands of nuclear species on the neutron-rich side of stability. One important nuclear quantity is the probability a nucleus will emit one or more neutrons following a  $\beta$  decay. Here we consider the role of  $\beta$ -delayed neutron emission in finalizing the pattern of isobaric abundances produced in  $r$ -process simulations. We focus on the sensitivity of the details of the abundance pattern to the  $\beta$ -delayed neutron emission probabilities of individual nuclei, for hot, cold, and neutron star merger  $r$ -process scenarios.

**KEYWORDS:**  $r$  process, beta decay, stellar elemental abundances

## 1. Introduction

The detailed pattern of abundances produced in rapid neutron capture, or  $r$ -process, nucleosynthesis depends upon the nuclear physics properties—masses,  $\beta$ -decay rates,  $\beta$ -delayed neutron emission probabilities, neutron capture rates, fission probabilities and daughter product distributions, and neutrino capture rates—of the thousands of unstable neutron-rich nuclear species that participate in the process; see, e.g., [1, 2] for recent reviews. Masses and  $\beta$ -decay rates are arguably the most important of these properties. In the classic picture of the  $r$  process, the nuclear flow proceeds in hot ( $T > 1$  GK), neutron-rich ( $n_n > 10^{22}$  g/cm<sup>3</sup>) conditions where an equilibrium is established between neutron captures and photodissociations [3, 4]. The abundances along an isotopic chain in this  $(n, \gamma)$ - $(\gamma, n)$  equilibrium are determined by the temperature and neutron density of the local conditions and the sequence of neutron separation energies along the chain.  $\beta$  decay connects the different isotopic chains and therefore sets their relative abundances.

Even in these early calculations, it was clear that an additional step was required to connect the abundances produced in equilibrium to the final abundance pattern obtained. The isotopes of maximum abundance in equilibrium have even neutron number  $N$  everywhere, due to the strength of the nuclear pairing force. As a result the equilibrium  $r$ -process abundances show a strong even-odd staggering, illustrated in Fig. 1. The solar pattern of  $r$ -process residuals, however, contains no such staggering.  $\beta$ -delayed neutron emission was invoked as the mechanism to smooth the equilibrium pattern [5, 6].

$\beta$ -delayed neutron emission is the prompt emission of a neutron following a  $\beta$  decay. It can occur when the decay populates a neutron-unbound excited state in the daughter, which is possible when the  $\beta$  decay  $Q$ -value  $Q_\beta$  exceeds the neutron separation energy  $S_n$  of the daughter nucleus. Close to stability this is unlikely to occur. However, far from stability the difference between  $Q_\beta$  and  $S_n$  can become quite large, and the emission of one to several

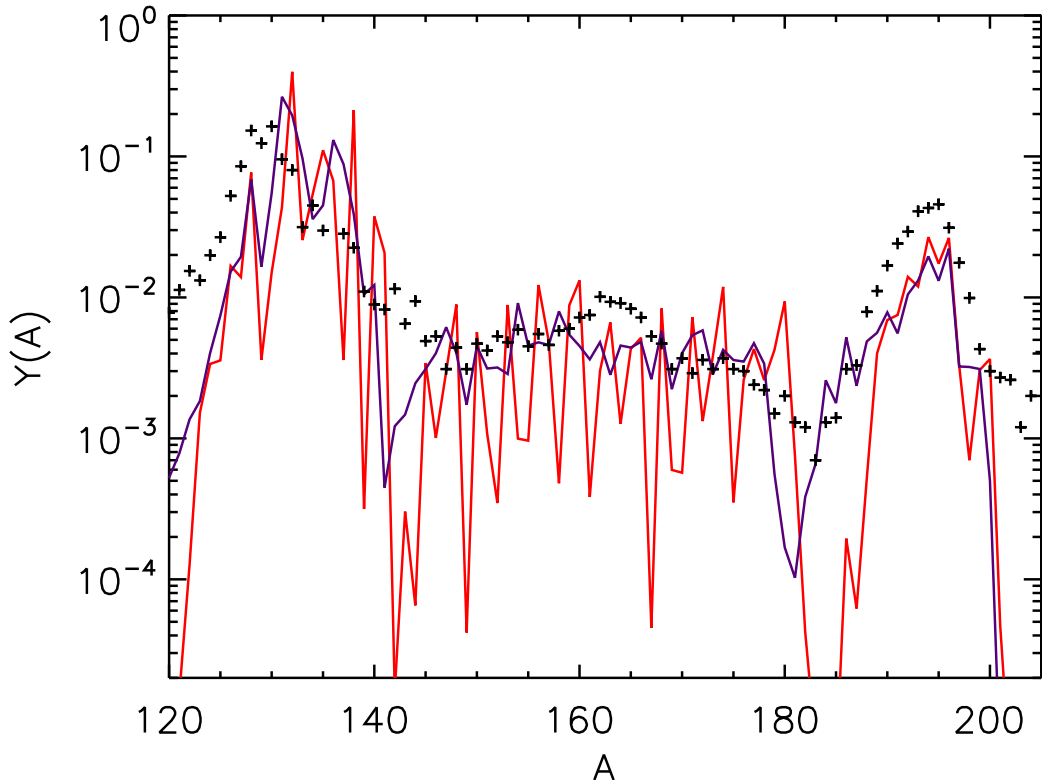


**Fig. 1.** Abundances  $Y(A)$  versus mass number  $A$  for a hot wind  $r$  process during  $(n, \gamma)$ - $(\gamma, n)$  equilibrium (red line) and after an instantaneous freezeout (purple line), scaled to compare to the solar  $r$ -process residuals [7]. The calculation of instantaneous freezeout from equilibrium includes only  $\beta$  decays and  $\beta$ -delayed neutron emission as material moves from the equilibrium  $r$ -process path to stability.

neutrons after decay is energetically favored. Thus, the very neutron-rich isotopes produced in an  $(n, \gamma)$ - $(\gamma, n)$  equilibrium will emit  $\beta$ -delayed neutrons on the decay paths to stability. In the classic picture of the  $r$  process, where equilibrium is followed by an instantaneous freezeout and decay to stability,  $\beta$ -delayed neutron emission is sufficient to significantly smooth the resulting abundance pattern [8,9]. An example of this is shown in Fig. 1.

Modern  $r$ -process simulations investigating realistic astrophysical environments employ fully dynamical nuclear networks [10, 11] with no assumption of  $(n, \gamma)$ - $(\gamma, n)$  equilibrium. These simulations show that in some environments  $(n, \gamma)$ - $(\gamma, n)$  equilibrium is indeed established, while in others it is established briefly if at all. When out of equilibrium, the  $r$ -process reaction flow is determined by individual rates of neutron capture,  $\beta$  decay, and photodissociation. Additionally the role played by  $\beta$ -delayed neutron emission is quite different than in the equilibrium-only scenario. In dynamical simulations, the odd-even staggering of the abundance pattern is primarily erased via neutron captures during freezeout [12]. An example of this is shown in the top panel of Fig. 2, which compares abundance patterns with and without  $\beta$ -delayed neutron emission for a fully dynamical hot wind  $r$ -process simulation. During the equilibrium phase of this simulation, the abundance pattern is identical to the red line of Fig. 1. After the freezeout phase, the abundances of the odd- $N$  isotopes are largely filled in regardless of whether  $\beta$ -delayed neutron emission is included.

In the dynamical picture of the  $r$  process,  $\beta$ -delayed neutron emission plays two roles:

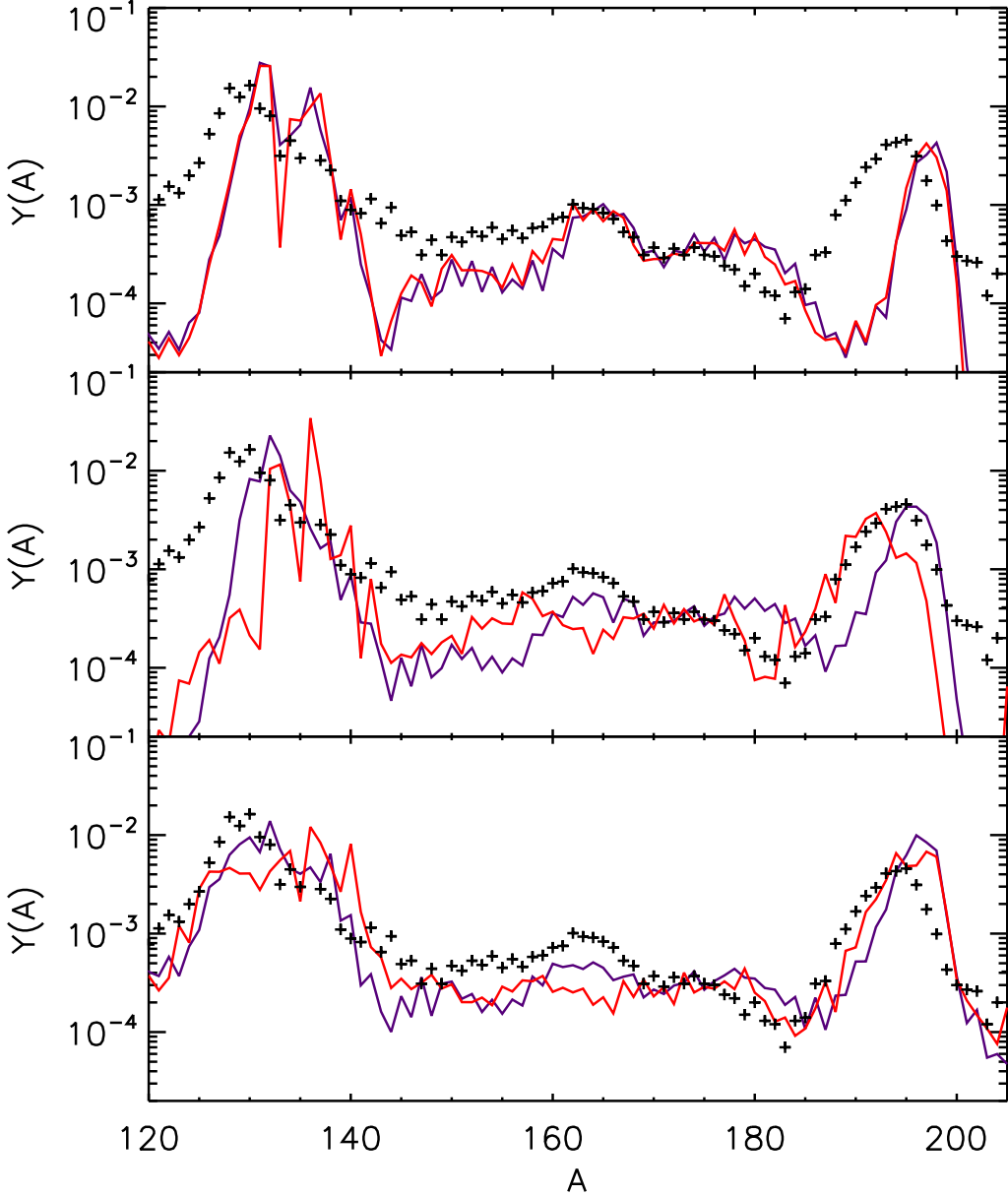


**Fig. 2.** Final abundances  $Y(A)$  versus mass number  $A$  for a hot wind parameterized as in [13] (with entropy  $s/k = 100$ , timescale  $\tau = 80$  ms, and initial electron fraction  $Y_e = 0.25$ ; top panel), a cold wind from [14] (with  $Y_e$  reduced to 0.31; middle panel) and a neutron star merger example from Bauswein and Janka as in [15] (bottom panel), for simulations where  $\beta$ -delayed neutron emission is included (purple lines) or omitted (red lines). Crosses show scaled solar  $r$ -process residuals from [7].

(1) as an important source of neutrons for late-time, non-equilibrium captures, and (2) in finalizing the fine details of the abundance pattern. The latter is clearly shown in the top panel of Fig. 2 for a hot  $r$ -process example. The middle panel of Fig. 2 contains an example of the former, where the final abundance patterns of a cold  $r$ -process simulation run with and without  $\beta$ -delayed neutron emission are compared. In a cold  $r$ -process [16], the temperature drops quickly and photodissociation becomes negligible. Without photodissociations to

counter neutron captures, the  $r$ -process path becomes very neutron rich and the neutrons are rapidly consumed. As the neutrons are depleted, the path moves back toward stability, and late-time neutron captures drive the formation of the rare earth peak at  $A \sim 165$  and can move the major peaks several units in  $A$ . Without the late-time neutrons provided by  $\beta$ -delayed neutron emission, the rare earth peak does not form and the main peak locations are markedly different. The bottom panel of Fig. 2 shows the same comparison for a neutron star merger example trajectory. Here, the conditions are so neutron rich that the  $r$ -process dynamics are dominated by fission recycling. Thus most of the late-time neutrons in this environment are supplied by fission. Still,  $\beta$ -delayed neutron emission does contribute to shaping the details of the final pattern, including the rare earth peak.

The probabilities for  $\beta$ -delayed emission of  $x$  neutrons,  $P_{xn}$ , used in  $r$ -process simulations are largely theoretical, as they have been measured for only a small handful of nuclei important for the  $r$  process. These few measurements suggest theoretical  $P_{xn}$  values are underestimates of the actual, e.g. [17]. To fully understand the contribution of  $\beta$ -delayed neutron emission as a source of late time neutrons, a better understanding of the systematics of  $P_{xn}$  values far from stability is needed for almost the entire nuclear chart. This will require progress in both experiment and theory.

Our aim here is to seed this progress by pointing out *individual*  $\beta$ -delayed neutron emission probabilities that influence  $r$ -process abundance patterns. A change to the  $P_{xn}$  value for a single nucleus is unlikely to alter the contribution of  $\beta$ -delayed neutron emission to the availability of late-time neutrons. However it can readjust the details of the final abundance pattern locally. In the next section we describe sensitivity studies that identify which  $P_{xn}$  values have the greatest impact on the abundance pattern produced in three types of astrophysical scenarios.

## 2. Sensitivity Studies

The sensitivity studies performed here are similar to recent studies of individual masses [18–21],  $\beta$ -decay rates [20, 22], and neutron capture rates [20, 23–25]. We start with a choice of astrophysical conditions and run a baseline  $r$ -process simulation. We then vary a single piece of nuclear data, rerun the simulation, and compare the result to the baseline with the sensitivity measure  $F$ :

$$F = 100 \times \sum_A |X(A) - X_{\text{baseline}}(A)| \quad (1)$$

where  $X_{\text{baseline}}(A)$  are the final mass fractions of the baseline abundance pattern and  $X(A)$  are the final mass fractions for the simulation with the nuclear data change.

Here, we report initial results for three  $\beta$ -delayed neutron emission sensitivity studies. The studies each begin with a distinct astrophysical scenario: a hot  $r$ -process wind, a cold  $r$ -process wind, and a neutron star merger trajectory. The hot wind is parameterized as in [13], with entropy per baryon  $s/k = 100$ , timescale  $\tau = 80$  ms, and initial electron fraction  $Y_e = 0.250$ . The cold wind is taken to be a trajectory from [14], where the initial electron fraction is dropped to 0.31 to yield a main  $r$  process. The neutron star merger trajectory is from Bauswein and Janka, as in [15]. We run all of the simulations with FRDM masses [26],  $\beta$ -decay rates from [27], and neutron capture rates from [28], and fission treated as in [29]. The abundance patterns of the baseline simulations are shown in Fig. 2.

For each nuclear data change, we set all of  $\beta$ -delayed neutron emission probabilities  $P_{xn}$ , for  $x \geq 1$ , to zero and  $P_{0n}$  to 1 for a single nucleus. Thus, the possibility of  $\beta$ -delayed neutron emission for that nucleus is turned off but the overall  $\beta$  lifetime is not altered. Fig. 3 shows an example of the abundance pattern changes that can result. Here the baseline cold  $r$ -process

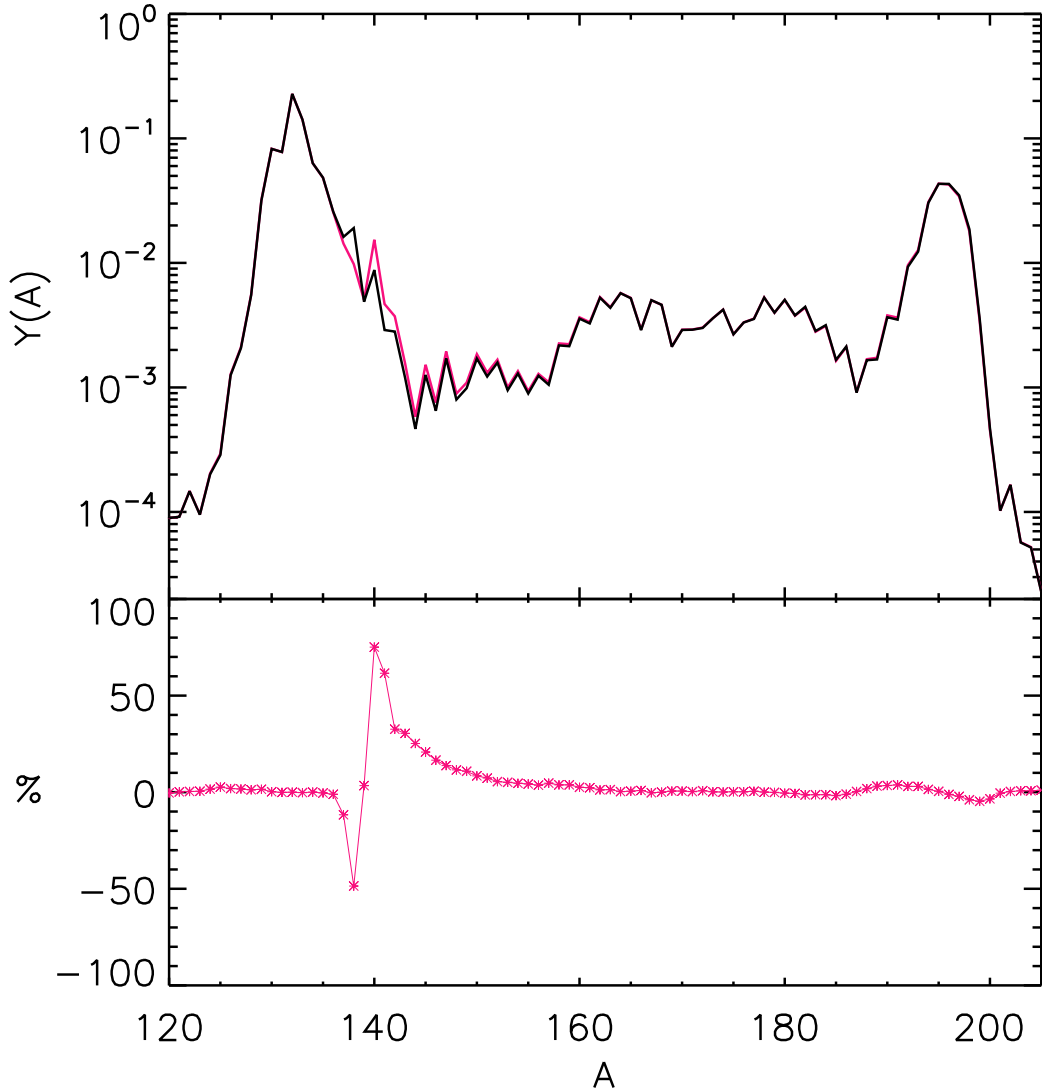


**Fig. 3.** Final abundances  $Y(A)$  versus mass number  $A$  for a cold wind  $r$ -process simulation where the  $\beta$ -delayed neutron emission probabilities for  $^{140}\text{Sn}$  are set to zero (pink) or kept at the theoretical values from [27] (black). The bottom panel shows the percentage difference between the two patterns.

abundance pattern is compared to the results of a simulation identical except the  $P_{xn}$  values of  $^{140}\text{Sn}$  are set to zero from their baseline FRDM values of  $P_{1n} = 0.8807$ ,  $P_{2n} = 0.0355$ , and  $P_{3n} = 0.0063$  [27]. The change to this one nucleus produces a sharp local change to the final abundance pattern as expected: a higher abundance for  $A = 140$  nuclei and lower for  $A = 138$  nuclei when  $r$ -process path nucleus  $^{140}\text{Sn}$   $\beta$  decays without emitting neutrons. The freezeout nuclear reaction flow in that region readjusts to this change, and smaller modifications to the abundances at slightly higher mass numbers result. Since the abundance pattern changes are largely local, the (global) sensitivity measure  $F$  calculated using Eqn. 1 is small; for this example it is 1.98.

The analysis described above is repeated for every nucleus with  $40 < Z < 80$  throughout the nuclear chart, for each of the three baseline simulations. Figs. 4-6 show the final  $F$  measures for each case. For the hot wind example, the sensitivities are limited to a narrow band of

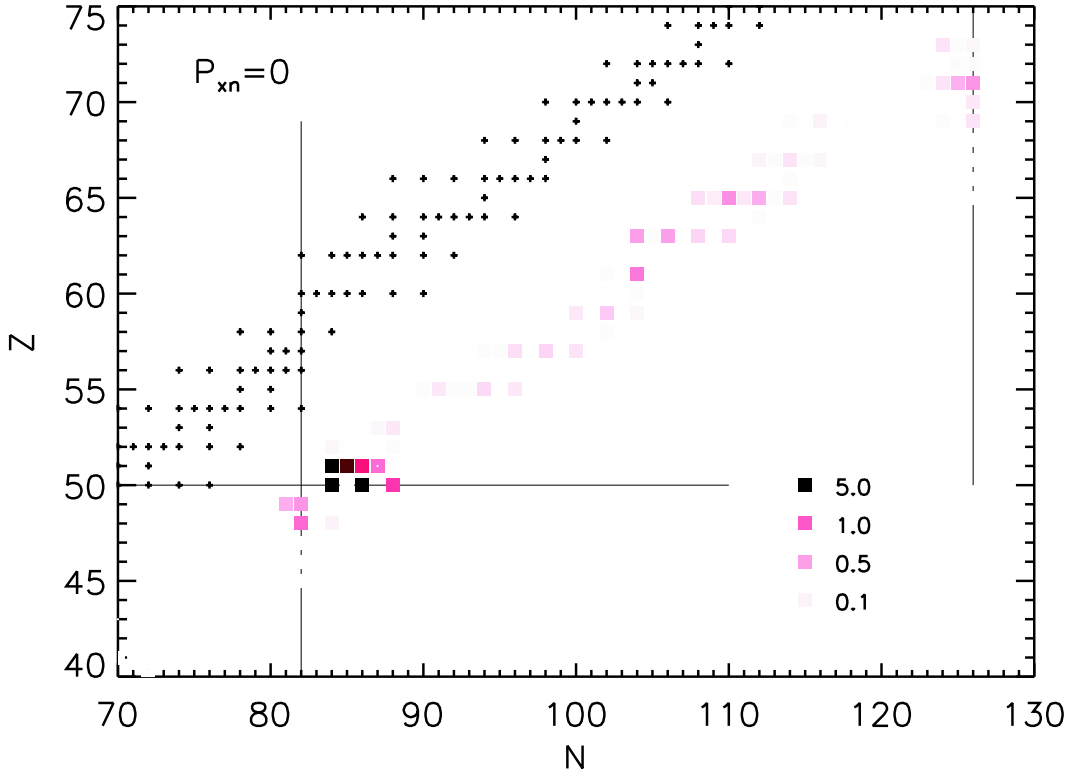


**Fig. 4.** Sensitivity measures  $F$  resulting from a sensitivity study in which  $\beta$ -delayed neutron emission is turned off for one nuclear species at a time. The baseline simulation is the hot  $r$ -process parameterized wind described in the text. The sensitivity measures are plotted on a continuous scale, with the darkest shading corresponding to  $F > 5$  and several intermediate values indicated in the key.

primarily even- $N$  nuclei. This is because individual  $\beta$ -delayed neutron emission probabilities only become important in freezeout, after most of the neutrons are exhausted and  $(n, \gamma)$ - $(\gamma, n)$  equilibrium has failed. The nuclei showing the largest sensitivity measures therefore tend to be those most populated during the decay back to stability. For the hot  $r$ -process case, the equilibrium path is neutron-rich but not extremely so, such that in freezeout the decay back to stability quickly reaches the region of the nuclear chart for which  $\beta$ -delayed neutron emission is not energetically allowed. For the cold  $r$ -process and merger cases, the  $r$ -process path is much farther from stability, so the  $\beta$ -delayed neutron emission probabilities of many more nuclei can have an impact. The most important  $P_{xn}$  values tend to be those of even- $N$  nuclei, with the highest  $F$  measures obtained for nuclei along the decay pathways of the  $N = 82$  and  $N = 126$  closed shell nuclei.

Note that here we have not investigated the influence of potential *increases* to  $P_{xn}$  values. We plan to address this along with several other improvements to these studies in an upcoming work.

### 3. Conclusion

$\beta$ -delayed neutron emission is of key importance in the late stages of the  $r$  process, as it provides neutrons for late-time, non-equilibrium captures and adjusts the fine details of the isobaric abundance pattern. We focus on the latter in the sensitivity studies described here,

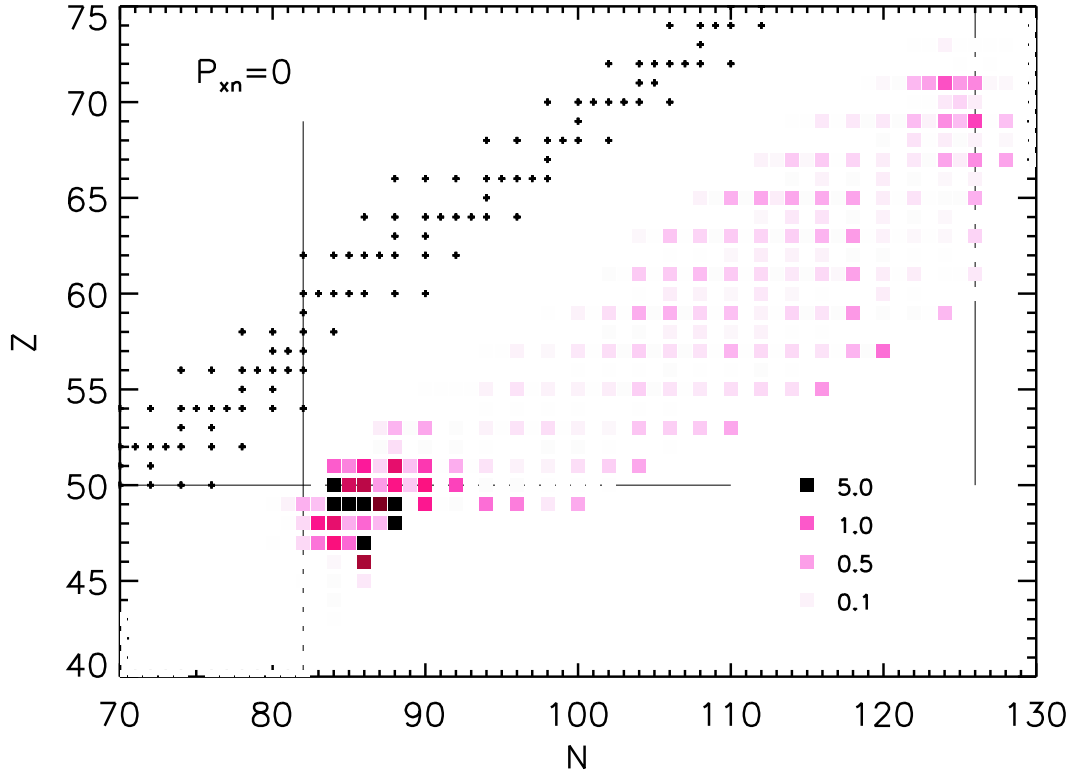


**Fig. 5.** Same as Fig. 4 for the cold wind example.

which point out the individual  $\beta$ -delayed neutron emission probabilities that have the greatest influence on the final abundance pattern. As is clear from Figs. 4–6 the range of nuclei whose  $P_{xn}$  values show up as important vary widely between the different astrophysical scenarios. However, even- $N$  nuclei 10–15 neutrons from stability are influential in all cases. Many of these nuclei, particularly near the  $N = 82$  closed shell, are within the reach of current and upcoming experimental campaigns at RIKEN [30], CARIBU [31] and GSI-FRS [32].

## References

- [1] M. Arnould, S. Goriely, and K. Takahashi: *Phys. Rep.* **450** (2007) 97.
- [2] F.-K. Thielemann, et al.: *Prog. Part. Nucl. Phys.* **66** (2011) 346.
- [3] E.M. Burbidge, G.R. Burbidge, W.A. Fowler, and F. Hoyle: *Rev. Mod. Phys.* **29** (1957) 547.
- [4] A.G.W. Cameron: *Chalk River Rep.* **CRL-41** (1957).
- [5] A.G.W. Cameron, M.D. Delano, and J.W. Truran: *CERN 70-30* **2** (1970) 235.
- [6] T. Kodama and K. Takahashi: *Nucl. Phys. A* **239** (1975) 489.
- [7] C. Sneden, J. Cowan, and R. Gallino: *Annu. Rev. Astro. Astrophys.* **46** (2008) 241.
- [8] W. Hillebrandt, K. Takahashi, and T. Kodama: *Astron. Astrophys.* **52** (1976) 63.
- [9] K.-L. Kratz, et al.: *Astrophys. J.* **403** (1993) 216.
- [10] J.J. Cowan, A.G.W. Cameron, and J.W. Truran: *Astrophys. J.* **265** (1983) 429.
- [11] J.J. Cowan, F.-K. Thielemann, and J.W. Truran: *Phys. Rep.* **208** (1991) 267.
- [12] D.N. Schramm: *Astrophys. J.* **185** (1973) 293.
- [13] B.S. Meyer: *Phys. Rev. C* **89** (2002) 231101.
- [14] A. Arcones, H.-Th. Janka, and L. Scheck: *Astron. Astrophys.* **467** (2007) 1227.
- [15] S. Goriely, A. Bauswein, and H.-Th. Janka: *Astrophys. J.* **738** (2011) L32.
- [16] S. Wanajo and Y. Ishimaru: *Nucl. Phys. A* **777** (2006) 676.

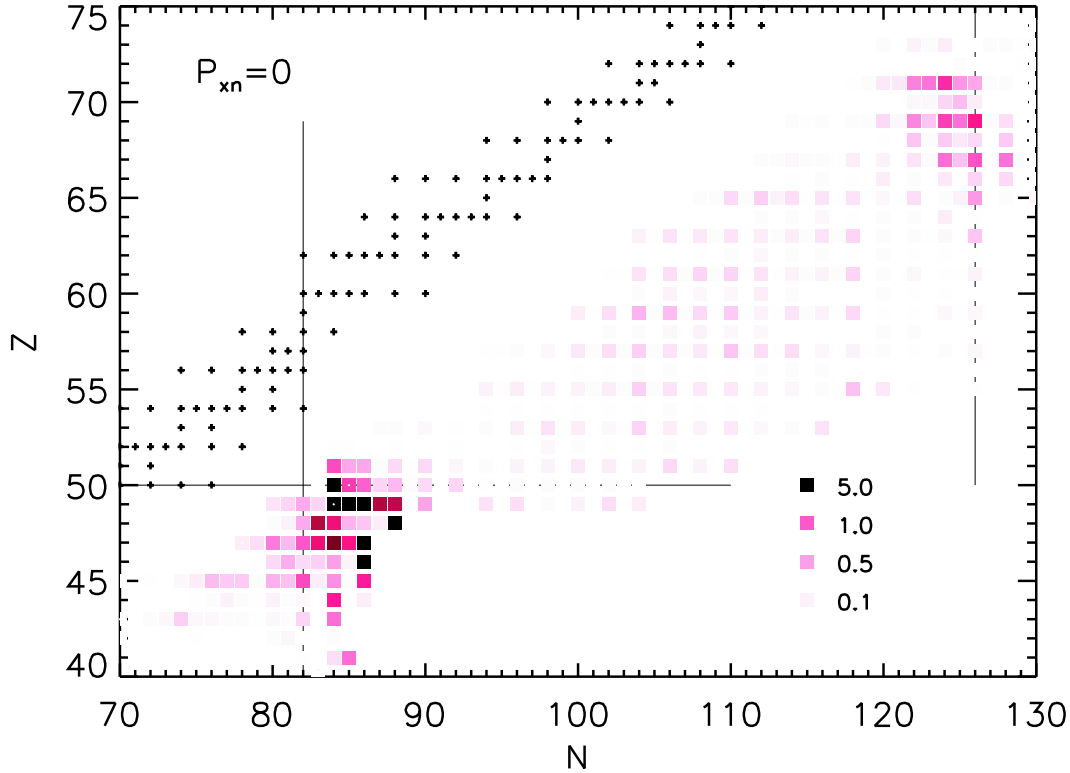


**Fig. 6.** Same as Fig. 4 for the neutron star merger example.

- [17] K. Miernik, et al.: Phys. Rev. Lett. **111** (2013) 132502.
- [18] S. Brett, I. Bentley, N. Paul, R. Surman, and A. Aprahamian: E. Phys. J. A **48** (2012) 184.
- [19] A. Aprahamian, I. Bentley, M. Mumpower, and R. Surman: AIP Advances **4** (2014) 041101.
- [20] R. Surman, M. Mumpower, J. Cass, I. Bentley, A. Aprahamian, and G.C. McLaughlin: European Physical Journal Web of Conferences **66** (2014) 7024.
- [21] M. Mumpower, D.-L. Fang, R. Surman, M. Beard, and A. Aprahamian, submitted (2014).
- [22] M. Mumpower, J. Cass, G. Passucci, R. Surman, and A. Aprahamian: AIP Advances **4** (2014) 041009.
- [23] R. Surman, J. Beun, G.C. McLaughlin, and W.R. Hix: Phys. Rev. C **79** (2009) 045809.
- [24] M. Mumpower, G.C. McLaughlin, and R. Surman: Phys. Rev. C **86** (2012) 035803.
- [25] R. Surman, M. Mumpower, R. Sinclair, K. L. Jones, W. R. Hix, and G. C. McLaughlin: AIP Advances **4** (2014) 041008.
- [26] P. Möller, J. R. Nix, W. D. Meyers, and W. J. Swiatecki: At. Data Nucl. Data Tables **59** (1995) 185.
- [27] P. Möller, B. Pfeiffer, and K.-L. Kratz: Phys. Rev. C **67** (2003) 055802.
- [28] T. Rauscher and F.-K. Thielemann: At. Data Nucl. Data Tables **75** (2000) 1.
- [29] J. Beun, G.C. McLaughlin, R. Surman, and W.R. Hix: Phys. Rev. C **77** (2008) 035804.
- [30] I. Dillmann, D. Abriola, and B. Singh: AIP Conference Proceedings **1594** (2014) 332.
- [31] N.D. Scielzo, et al.: Nuclear Data Sheets **120** (2014) 70.
- [32] R. Caballero-Folch, et al.: Nuclear Data Sheets **120** (2014) 81.